Oxidation state localized orbitals: A method for assigning oxidation states using optimally fragment-localized orbitals and a fragment orbital localization index

Martí Gimferrer[#,†] Abdulrahman Aldossary[#,‡] Pedro Salvador,[*,†] and Martin Head-Gordon[*,‡]

†*Institut de Química Computacional i Catàlsi and Departament de Química, Universitat de Girona, 17003 Girona, Catalonia, Spain*

‡ *Pitzer Center for Theoretical Chemistry, Department of Chemistry, University of California, Berkeley CA 94720*

E-mail: pedro.salvador@udg.edu; mhg@cchem.berkeley.edu

[#] These authors made equal contributions

Abstract

Oxidation states represent the ionic distribution of charge in a molecule, and are significant in tracking redox reactions and understanding chemical bonding. While effective algorithms already exist based on formal Lewis structures, as well as using localized orbitals, they exhibit differences in challenging cases where effects such as redox non-innocence are at play. Given a density functional theory (DFT) calculation with chosen total charge and spin multiplicity, this work reports a new approach to obtaining fragment-localized orbitals that is termed oxidation state localized orbitals

(OSLO), together with an algorithm for assigning the oxidation state using the OSLOs and an associated fragment orbital localization index (FOLI). Evaluating the FOLI requires fragment populations, and for this purpose a new version of the intrinsic atomic orbital (IAO) scheme is introduced in which the IAOs are evaluated using a reference minimal basis formed from on-the-fly superposition of atomic density (IAO-AutoSAD) calculations in the target basis set, and at the target level of theory. The OSLO algorithm is applied to a range of challenging cases including high valent metal oxide complexes, redox non-innocent NO and dithiolate transition metal complexes, a range of carbene-containing TM complexes, and other examples including the potentially inverted ligand field in $[Cu(CF_3)_4]^-$. Across this range of cases, OSLO produces generally satisfactory results. Furthermore, in borderline cases, the OSLOs and associated FOLI values provide direct evidence of the emergence of covalent interactions between fragments that nicely complements existing approaches.

Introduction

The oxidation state (OS)[1] is a venerable concept reaching back to the early days of chemistry where the "oxydationsstufe" was introduced to rationalize the products obtained from reactions with oxygen. The electron-gathering tendency of oxygen is captured via its normal OS of -2 in compounds with ionic interactions, which is but one of the generally accepted counting rules to assign the OS. After a thorough revision of the concept, the IUPAC defines the OS of an atom as the charge of this atom after ionic approximation of its hetero-nuclear bonds.[2] They further recommend that this is accomplished by writing the Lewis structure of the compound of interest, and partitioning the electron pairs such that each shared electron pair is given to the more electronegative of the two associated atoms.[3] The IUPAC procedure is simple and generally effective, and for these reasons should be the first resort in assigning OSs in new compounds of interest.

While the OS is a chemical concept of enduring value, it must be stressed that never-

theless, the OS of an atom is not itself a precisely defined observable. It *may* correlate with observables such as x-ray absorption spectral shifts, but this requires calibration. Ultimately, the validity of the OS depends on the extent of ionicity in the bonding. Thus the OS becomes less well-defined as the chemical bonding approaches the covalent limit of electron pair sharing. Other situations such as ligand non-innocence[4] also can defeat normal OS conventions. Indeed the IUAPC report on OSs in chemistry states that there are "limits, beyond which OS ceases to be well-defined or becomes ambiguous". This situation is no different than other valuable chemical concepts such as aromaticity,[5–7] and should not be viewed as a reason to discard the OS as something that cannot be measured. Instead, it is a reason to have tools that go beyond electron counting to assess the electron distribution in interesting and challenging borderline cases.

Electronic structure calculations directly yield the electron density, and therefore offer an ideal starting point for probing the borderline cases. Thus the assignment of OSs in molecular systems has drawn continuing attention in recent years.[8–16] Beyond the electron density itself, there is particular interest in the development and application of specific schemes to extract OSs from electronic structure calculations, going beyond the (simple but clearly not satisfactory) use of partial atomic charges or atomic spin densities.[17–20] Most electronic structure approaches to OS assignment are predicated on assigning each electron pair (or individual electrons in case of open-shell systems) to one atom or ligand within the system based on some strategy that generalizes simple counting approaches such as the IUPAC definition. While we will concentrate on molecular systems in this work, it must be mentioned that precisely the same issue exists for oxidation state assignments in solid state materials.[21–23]

Some years ago, Ramos-Cordoba et al. introduced a general OS elucidation method applicable to any molecular system and wavefunction (single-determinant or correlated)[19] that relies on Mayer's effective fragment orbitals (EFOs) and their occupations.[24,25] The EFOs are obtained by diagonalization of the fragment's density matrix, according to some atom-

in-molecule definition. For instance, in the case of QTAIM they lie spatially within the fragment's boundary, so they represent natural domain orbitals. The spin-resolved EFOs are obtained independently for each user-defined fragment (typically the transition metal (TM) and its ligands). They are sorted by decreasing occupation number, and electrons (or electron pairs for closed-shell systems) are assigned to them until one reaches the total number of electrons. The fragment OS is then obtained by subtraction from the corresponding nuclear charges. This effective oxidation states (EOS) analysis, also provides a measure to quantify the extent to which the OS assignment is clear-cut, based on the difference in occupancy between the last occupied and first unoccupied EFOs. EOS analysis has been successfully applied to a wide range of systems.[26] The method notably deviates from the IUPAC approach[2,3] because individual bonds are never explicitly considered. That permits EOS analysis to formally consider more than one Lewis structure at a time (i.e. treat multireference wavefunctions) on an equal footing.

Single-determinant wavefunctions are invariant to unitary transformations within the occupied molecular orbitals. While the canonical orbitals are typically delocalized (because they are appropriate for ionization), this invariance can be exploited to generate a set of localized orbitals (LO) based on some criterion.[27] This is directly possible within Kohn-Sham density functional theory (DFT), which is the dominant electronic structure approach.[28] The LO representation often produces orbitals that resemble the individual bonds in the dominant Lewis structure, and it is then natural to apply the ionic approximation to each LO individually, following the IUPAC definition more closely. However, since there is no unique way to define localization, there is a slew of different localization schemes to produce localized orbitals, namely Boys[29] Pipek-Mezey (PM),[30] Edminston-Ruedenberg (ER),[31] or more recent realizations based on Cholesky decomposition of the density matrix[32] and the fourth moment[33] or Knizia's intrinsic bond orbitals (IBOs),[34] to name a few.

This avenue has been explored by a number of methods.[17,18,20] Thom et al[17] first coupled orbital localization with population analysis in the localized orbitals bonding analysis

(LOBA) to assign the electrons associated with each LO. The LOBA method starts with orbital localization by a chosen scheme, and then obtains the atomic populations from each localized orbital. Using either PM or ER localization together with Löwdin population analysis produced quite robust results.[10,17] In the original paper, the OS assignment focused on the TM of the complex. A threshold of 60% in the atomic population was used to decide whether the electron pair is assigned to the TM or not. Recently, some of us[35] described an extension to the method, loosening the weight of the aforementioned threshold in the OS determination, to allow the possibility of covalent assignment (split between two atoms/fragments), and introducing a confidence measure for the assignment (either ionic or covalent) of each electron pair.

In that work[35] we observed that for some of the most challenging systems such as TM-carbenes, the LOBA method struggled to reach the accepted OS. Careful inspection of the localized orbitals indicated that the first step of the procedure, namely the orbital localization, was not always producing orbitals one could easily relate to a Lewis structure. The LOs often involve several atomic centers with appreciable contributions, which hinder the process of OS assignment. Moreover, using a different localization scheme could also lead to different OS assignments in some controversial cases. We concluded that a different orbital localization scheme, tailored for the purpose of OS assignment, was necessary to make progress in such cases.

A maximally robust procedure to assign OSs should rely on separating the localized orbitals into fragments, for which the degree of locality of core or valence orbitals *within* each fragment has no special relevance. Indeed there has been much development of specialized methods that aim to specifically localize orbitals onto fragments[36–44] rather than maximizing a global measure of localization. Such methods have considerable value in energy decomposition analysis of intermolecular interactions,[45,46] as well as for fragment methods and embedding.[41,44,47] In our context there is a different need for fragment localization. For instance, if two fragments A and B, each formally bearing n_{A} and n_{B} electron pairs, are linked

via a single bond with ionic character, then the OS should solely depend on a single localized orbital involving both A and B, leading either to A^+-B^- or A^--B^+. On the other hand, since standard *system-optimal* orbital localization schemes do not make a distinction between the contact atoms of the A-B bond and the remaining atoms of A and B, a potentially better localization of the critical A-B bonding orbital may be sacrificed for better overall localization of all $n_A + n_B$ orbitals.

In light of the above considerations, there are several new components that are presented here to enable assignment of OSs. First, we put forward a robust fragment-based orbital localization scheme. For a given fragment, the resulting oxidation state localized orbitals (OSLOs) comprise a full set of orbitals spanning the occupied space that are ordered by spatial locality in the fragment. Second, to further characterize each orbital, given a set of fragment populations, we introduce a Fragment Orbital Localization Index (FOLI) which measures the population of each OSLO on a per-fragment basis. Third, to obtain the fragment populations, a more robust Hilbert-space based population analysis based on Knizia's intrinsic atomic orbitals (IAOs)[34] is also introduced. Fourth, we use the above components to develop an iterative algorithm to best select a *subset* of the OSLOs for each fragment to span the full occupied space. The oxidation state of a given fragment is then determined by its number of assigned OSLOs relative to its total nuclear charge. Finally, with the new procedure in hand, we turn to exploration of a variety of interesting borderline cases, with focus on examples where LOBA was previously demonstrated to have some issues.[35]

Methods

Oxidation States from Localized Orbitals (OSLO)

Starting with a single-determinant wavefunction built of n_{occ} spin orbitals, the fragment localization procedure is based on minimizing the radial spread functional from a given reference point for fragment F, $\mathbf{R}_F$. For a TM atom, $\mathbf{R}_F$ will be the atomic position; for a

ligand, $\mathbf{R}_F$ will be its center of charge or charge. The minimization can be easily achieved in the molecular orbital (MO) basis by building a spread matrix, $\mathbf{L}^F$, with elements

$$L_{ij}^F = \int \psi_i(\mathbf{r})(\mathbf{r} - \mathbf{R}_F)^2 \psi_j(\mathbf{r}) d\mathbf{r}, \tag{1}$$

where ψ_i is the i^{th} occupied MO. Equation 1 simplifies to

$$L_{ij}^F = \int \psi_i(\mathbf{r})\mathbf{r}^2\psi_j(\mathbf{r})d\mathbf{r} - 2\mathbf{R}_F \cdot \int \psi_i(\mathbf{r})\mathbf{r}\psi_j(\mathbf{r})d\mathbf{r} + \mathbf{R}_F^2\delta_{ij}, \tag{2}$$

where the first term contains the isotropic quadrupole moment matrix elements, the second term involves the dipole matrix elements, and the third term is a merely a constant diagonal offset. The required matrix elements are readily available in many quantum chemistry software packages. Diagonalization of the matrix $\mathbf{L}^F$

$$\mathbf{L}^F\mathbf{U}^F = \mathbf{U}^F\mathbf{\Lambda}^F \tag{3}$$

yields eigenvalues $\lambda_i^F = \Lambda_{ii}^F$ and a corresponding set of n_{occ} localized orbitals centered around $\mathbf{R}_F$

$$\phi_i^{loc,F}(\mathbf{r}) = \sum_k U_{ki}^F \psi_k(\mathbf{r}), \tag{4}$$

with their (squared) spreads given by the λ_i^X values. When $\mathbf{R}_F$ corresponds to an atomic position, the localized orbitals obtained by this procedure reproduce the shell structure of the atom, with core orbitals having the smaller spread values.

The target is to define the OS of M user-defined fragments of a molecular system, such as the metal(s) and ligands of a TM complex. We localize around each fragment's center of nuclear charge and get n_{occ} OSLOs for each of them (Mn_{occ} altogether). Note that in cases like polydentate or hapto ligands the ligand's centroid may be far from the ligand's nuclei, or even coincide with that of the metal (e.g. TM-porphyrin compounds). Minimizing the spread function is simple, non-iterative (no multiple minimum problem[48]), independent

of any population assignment, and appealing. However, the OSLOs most strongly associated with a fragment cannot always be chosen based on the smallest spread. For instance, in the case of a TM center with some coordination sphere, OSLOs dominated by ligand contributions can exhibit lower orbital spreads than the most diffuse TM orbitals (e.g. a 4s-type orbital for a 3d metal). Similarly, when $\mathbf{R}_F$ is the center of a ligand, some compact ligand-centered OSLOs have a significant contribution from the neighboring TM center.

We therefore need a complementary measure to identify those OSLOs that are most localized on a fragment. Using Pipek's delocalization measure,[49] defined in terms of *fragment populations*, $N_F^i = \sum_{A \in F} n_A^i$, rather than atomic populations, n_A^i, is a suitable starting point:

$$D_i = \{\sum_F (N_F^i)^2\}^{-1}, \tag{5}$$

When an orbital is localized on a single fragment, then $D_i = 1$. If the i^{th} orbital is perfectly delocalized across two fragments F and F' then $N_F^i = N_{F'}^i = 1/2$ and $D_i = 2$, and so on.

Out of the OSLOs generated from fragment F with low delocalization measure, we are interested in those that are also highly localized on fragment F. For this purpose, we introduce the fragment orbital localization index (FOLI)

$$D_i^F = \sqrt{\frac{D_i}{N_F^i}}, \tag{6}$$

The FOLI, D_i^F, is 1 when orbital i is perfectly localized on that fragment ($D_i = N_F^i = 1$). The FOLI $D_i^F \to 2$ when the orbital is perfectly delocalized over two fragments ($D_i = 2, N_F^i = N_{F'}^i = 0.5$). The FOLI gradually increases for OSLOs that are more delocalized and less centered on fragment F. Note that while a FOLI value of $D_i^F = 1$ means perfect fragment localization, higher FOLI values can result from different instances of delocalization. For example a FOLI value of 2 can also arise from 3 fragments with $D_i = 2.339$ via $N_F = 0.584$, $N_{F'} = N_{F''} = 0.208$.

How should one select the n most fragment-localized OSLOs from amongst the redundant

set of $M \cdot n$ candidates? One could select the n_{occ} OSLOs with the smallest FOLI values and assign them to their parent fragments. However, we have observed that this procedure sometimes leads to linear dependencies among the selected OSLOs. We instead prefer the iterative scheme depicted in Fig. 1. On the first iteration, the best localized orbital (in the sense of smallest FOLI value) is selected and projected out from the occupied space for the next iteration. The 2nd iteration begins by constructing a new set of $M \cdot (n_{\mathrm{occ}} - 1)$ localized orbitals, followed by selecting and removing the best localized orbital. Iterations continue until a total of n_{occ} optimal fragment-localized orbitals are selected. In the case of an unrestricted Slater determinant, the procedure is carried out for the α and β occupied spaces separately, and individual α and β OSLOs are thus produced and assigned to each fragment.

The basic algorithm is modified by introducing a tolerance (typically 10^{-3}) associated with the lowest FOLI values so that all OSLOs with D_i^F values within the tolerance are selected in a given iteration. These orbitals are symmetrically orthogonalized and then projected out from the occupied space for the next iteration. This strategy avoids the problem that for symmetric systems, projecting out individual localized orbitals may result in a symmetry-broken density-matrix for the next iteration.

There are a number of aspects of the procedure that are worth discussing in some detail. The localized orbitals obtained in the first few iterations are basically the atomic core orbitals of the fragment's atoms. As the iterative process advances, on-fragment localized valence orbitals are produced. They correspond to orbitals not particularly involved in the bonding between fragments, i.e. spectator orbitals. In the later iterations, the least-fragment localized valence orbitals are eventually selected. They correspond to bonds (or dative bonds) between fragments (e.g. TM-ligand orbitals). A nice side effect of the iterative procedure is that, by first removing the more fragment-localized orbitals from the occupied space, the relevant across-fragment orbitals are better localized on fragments (i.e. their FOLI values are *smaller* than those obtained in the first iteration using the whole occupied space). The final result

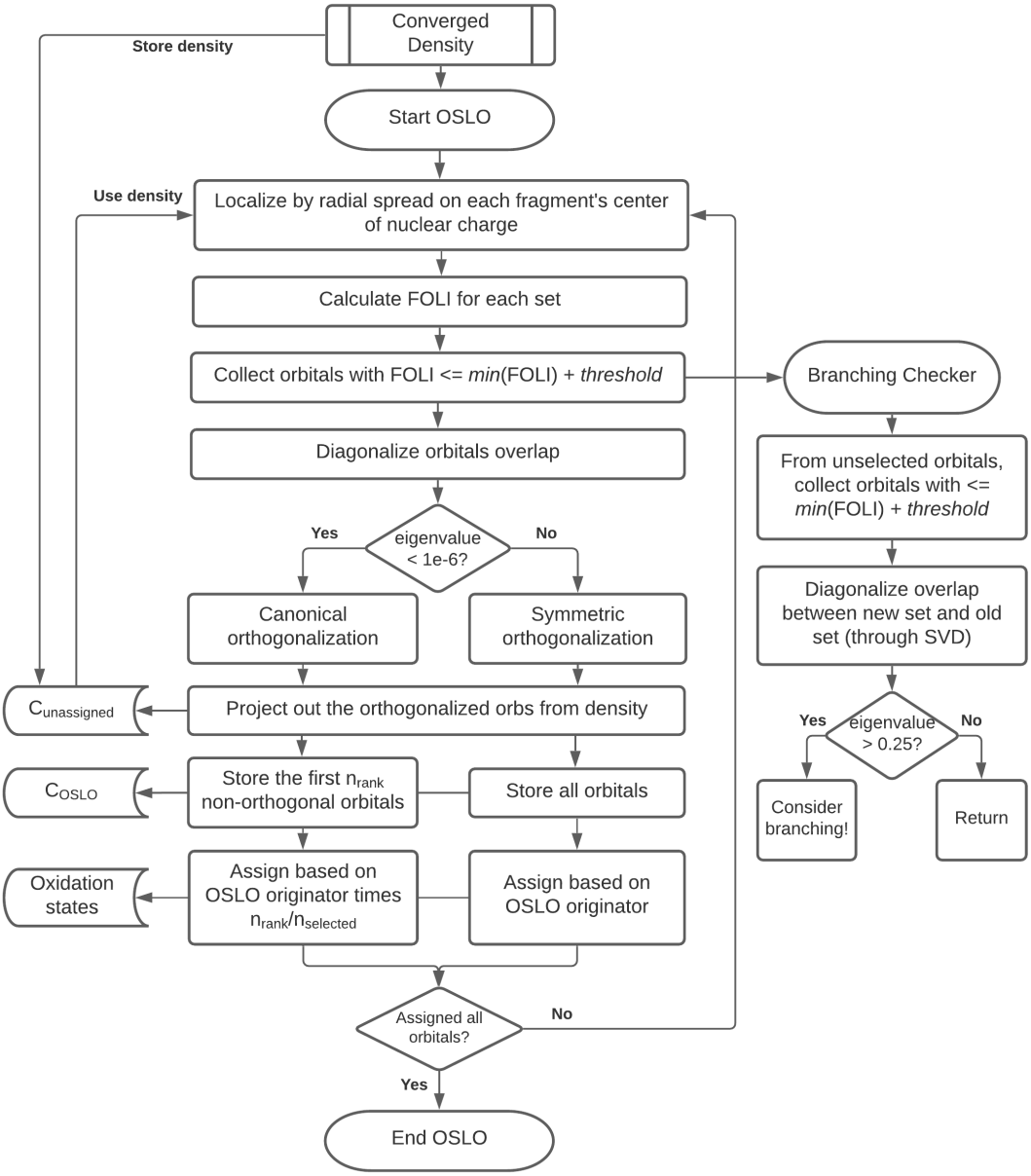

Figure 1: Flowchart of the iterative OSLO algorithm, where the most strongly fragment-localized orbitals (core and valence spectator orbitals) are projected out from the occupied space before the least fragment-localized orbitals that are most relevant to OS assignment are generated and inspected. This procedure has the desirable side-effect of improving the fragment-localization of orbitals that are not selected on later iterations.

thus depends to some extent on the order in which OSLOs are selected.

In borderline cases (where the FOLI-based selection is a close call) this may affect OS assignment. The algorithm allows the user to explore alternative outcomes in borderline cases by flagging when the OSLO selection procedure could *branch* into 2 (or more) paths. Consider a simple case with a single bond between fragments F and G. At some point in the iterative procedure, the corresponding bond localized orbital centered on F will be produced. At the same time, a similar bond localized orbital will be produced in the OSLOs associated with fragment G. The one with the smaller FOLI value is selected and projected out from the remaining occupied space. In the following iteration, this bond orbital will be absent from the new set of OSLOs obtained for both fragment F *and* G. If the $F-G$ bond is very non-polar (rare in TM complexes), the D_i^F and D_i^G values would be very similar, and one can argue that instead choosing the OSLO associated with G would produce a plausible alternative solution to selecting the one associated with F.

Our iterative algorithm automatically detects these (borderline) cases as follows. At each iteration, linear dependencies are checked between the OSLO that is selected and that with the *second* smallest FOLI value that is not selected (there may be multiple selected and non-selected localized orbitals if their FOLI values are within the tolerance). If near linear dependencies are indeed found *and* the difference in D_i^F values is small enough, our algorithm will print a diagnostic message. This allows the user to rerun the calculation, toggling a branching flag that selects the OSLO with the somewhat larger FOLI value, and proceed to obtain a second distinct solution.

To turn to OS assignment, we recall that each of the selected localized orbitals was generated from a fragment center with a low FOLI value. This makes it natural to assign the fragments' oxidation states based on the originator fragment. That is the procedure followed in the results reported here, and represents a "winner-takes-all" approach to the OS, similar to the IUPAC rules. However, once the optimal set of orthogonal fragment-localized orbitals are obtained, each orbital's allegiance may be reassigned according to

the fragments' populations, either in a "winner-takes-all" fashion again, or alternatively by allowing covalent assignments in non-polar cases, as described elsewhere.[35]

An atomic partitioning scheme is necessary to evaluate the FOLI values. In this work, we use two very different partitioning approaches to demonstrate that different reasonable choices in fact work very similarly. First, we use the so-called Topological Fuzzy Voronoi Cells (TFVC) atomic definition,[50] a real-space scheme that is used in the effective oxidation states (EOS) approach.[19] Second, we introduce a Hilbert-space based procedure based on Knizia's intrinsic atomic orbitals (IAOs),[34] where the reference minimal basis is obtained on-the-fly at the chosen level of theory. This IAO-AutoSAD procedure is described below.

The IAO-AutoSAD Reference Minimal Basis

Hilbert-space methods to assign atomic or fragment populations so that the results do not artificially depend on the underlying AO basis set often rely on using a minimal basis to *exactly* span the occupied space.[51–53] Amongst many such possibilities, Intrinsic Atomic Orbitals (IAOs) are perhaps the simplest, and have been shown to be robust for population analysis.[34,44,54] The basic idea of IAOs is to rely on a projection onto a reference minimal basis to facilitate atom-tagging.

Starting from a converged SCF solution, one projects the occupied MO coefficients, $\mathbf{C}_{\mathrm{occ}}$, into the small reference minimal basis set and back to the big one as follows:

$$\tilde{\mathbf{C}}_{\mathrm{occ}} = \mathrm{ortho}(\mathbf{R}_{\mathrm{ls}}\mathbf{R}_{\mathrm{sl}}\mathbf{C}_{\mathrm{occ}}), \tag{7}$$

$\mathbf{R}_{\mathrm{sl}} = \mathbf{s}^{-1}\mathbf{S}_{\mathrm{sl}}$ projects from the big basis into the small basis, given that $\mathbf{S}$ and $\mathbf{s}$ are the overlap matrices in the large and small basis sets, and $\mathbf{S}_{\mathrm{sl}}$ is the matrix of overlaps between functions in the small and large basis sets. In the same notation, $\mathbf{R}_{\mathrm{ls}} = \mathbf{S}^{-1}\mathbf{S}_{\mathrm{ls}}$ projects from the small basis into the big basis. After symmetric orthogonalization to restore orthonormality, the so-called de-polarized orbitals are gathered in the matrix $\tilde{\mathbf{C}}_{\mathrm{occ}}$.

The rectangular transformation matrix, $\mathbf{A}$, from the large basis, $\{\omega_\mu\}$, to the minimal IAO basis, $\chi_\alpha^{\mathrm{IAO}} = \sum_\mu \omega_\mu A_{\mu\alpha}$, is produced by the following double projection step:

$$\mathbf{A}_{\mathrm{ls}} = \mathrm{ortho}(\mathbf{P}\mathbf{S}\tilde{\mathbf{P}}\mathbf{S}_{\mathrm{ls}} + \mathbf{Q}\mathbf{S}\tilde{\mathbf{Q}})\mathbf{S}_{\mathrm{ls}}) \tag{8}$$

$\mathbf{P} = \mathbf{C}_{\mathrm{occ}}\mathbf{C}_{\mathrm{occ}}^\dagger$ and $\tilde{\mathbf{P}} = \tilde{\mathbf{C}}_{\mathrm{occ}}\tilde{\mathbf{C}}_{\mathrm{occ}}^\dagger$ are the density matrices (i.e. occupied projectors) associated with the original occupied MOs and the de-polarized occupied MOs, respectively. Their orthogonal complements are $\mathbf{Q} = \mathbf{S}^{-1} - \mathbf{P}$ and $\tilde{\mathbf{Q}} = \mathbf{S}^{-1} - \tilde{\mathbf{P}}$. Once the orthogonal IAOs are available, the IAO atomic population of atom B is obtained as

$$N_B = \sum_{\beta \in B} \left(\mathbf{P}^{\mathrm{IAO}}\right)_{\beta\beta} = \sum_{\beta \in B} \left(\mathbf{A}^\dagger \mathbf{S}\mathbf{P}\mathbf{S}\mathbf{A}\right)_{\beta\beta}. \tag{9}$$

The reference minimal basis originally used[34] for construction of the IAOs is the co-called "MinAO" set, which is the standard cc-pVTZ AO basis manually truncated to a minimal basis. When the molecular calculation uses effective core potentials (ECPs), "MinAO-PP" was employed, which is cc-pVTZ-PP truncated to a minimal basis (i.e. excluding core AOs). However, this reference minimal basis fails to be valid for ECPs of other sizes (i.e. larger or smaller core). These limitations that result from the MinAO reference minimal basis are particularly relevant when dealing with transition metals and heavier elements.

A universally applicable reference minimal basis is made on-the-fly from appropriate free atom density matrices obtained with the same functional and basis set as the molecular calculation. This is done using Q-Chem's[55] so-called AutoSAD functionality, which is normally employed to construct superposition of atomic density (SAD) initial guesses for DFT calculations at the target level of theory. Sphericalization is necessary to ensure proper shell structure in the reference minimal basis, since many atoms have partly occupied degenerate orbitals. For simplicity as well as to avoid ambiguity, we use the ground state of the neutral atom, although for some atoms, a case can be made for using different spin or charge states. For open shell atoms, the unrestricted SCF equations are solved, and the resulting α and β

density matrices are spin-averaged as well as sphericalized.

The IAO-AutoSAD procedure first solves the following generalized eigenvalue problem separately for each free atom, A:

$$\mathbf{P}^A \mathbf{c}_\alpha^A = \mathbf{S}^A \mathbf{c}_\alpha^A \lambda_\alpha \tag{10}$$

Each matrix is defined in the full basis of the free atom (rank n_A), and $\mathbf{P}^A$ is the sphericalized and spin-averaged density matrix. The reference minimal basis set on atom A is defined by choosing m_A orbitals, corresponding to the fully and fractionally occupied atomic orbitals (with $\lambda_\alpha \geq \frac{1}{14}$, such that the f shell is selected even for a cerium atom with a single f electron). The set of selected column vectors $\{\mathbf{c}_\alpha^A\}$ defines an $n_A \times m_A$ transformation to the MBS, $\mathbf{C}_{\mathrm{MBS}}^A$. The reference minimal basis has rank $M = \sum_A m_A$ with functions defined by the direct sum of the atomic transformations:

$$\mathbf{T} = \bigoplus_A \mathbf{C}_{\mathrm{MBS}}^A \tag{11}$$

Given the $N \times M$ transformation from the AO basis to the reference minimal basis, $\mathbf{T}$, all quantities needed to evaluate the IAOs with this MBS are available. For instance, referring back to Eqs. 7 and 8, we see that $\mathbf{s} = \mathbf{T}^\dagger \mathbf{S} \mathbf{T}$ and $\mathbf{S}_{\mathrm{sl}} = \mathbf{T}^\dagger \mathbf{S}$.

One must be aware that IAO orbitals and atomic charges do depend on the underlying choice of reference minimal basis. Fortunately, our IAO-AutoSAD procedure shows results that are generally very similar to using MinAO for problems where the latter can be applied (i.e. no pseudopotentials). Some examples are shown in Figure 2, for a wide range of AO basis sets. This is encouraging, and sets the stage for the results we report for the OSLO procedure in the following section. However, IAO charges do exhibit some dependence on the reference minimal basis. For instance, the O atomic charge in H_2O changes by $0.25e^-$ when using STO-3G as the reference minimal basis instead of MinAO or AutoSAD. For IAO-AutoSAD applied to transition metals, the choice of atomic state also has an impact. These issues may deserve further study in the future, as IAOs become more widely used.

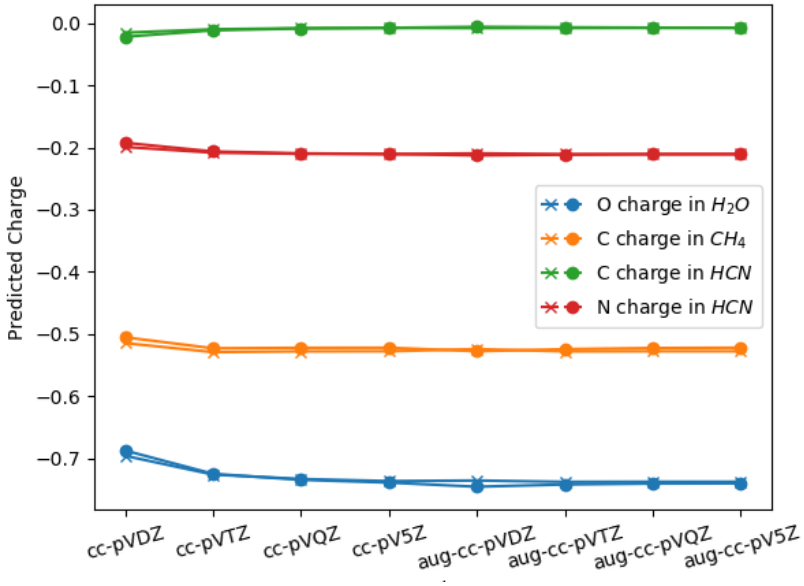

Figure 2: IAO atomic charges for H_2O, CH_4, and HCN where the crosses are charges from calculations using the AutoSAD reference minimal basis, while the circles used the MinAO basis.[34] All calculations are done with Hartree-Fock wavefunctions, and it is evident that the two sets of results are nearly indistinguishable.

Implementation and Computational Details

We have completed two independent implementations of the OSLO method, which serves as validation that both are correct, and also provides the opportunity to employ two different approaches to evaluate the fragment populations. Adopting the IAO-AutoSAD Hilbert space approach to charges described above, one of our implementations of the OSLO method is within the Q-Chem program package,[55] and consequently uses OSLO fragment populations and FOLI values that are obtained analytically. Our second implementation uses the Topological Fuzzy Voronoi Cells (TFVC) real-space atomic definition,[50] within the APOST-3D[56] package. The numerical evaluation of the TFVC charges used the atom-centered Becke multicenter quadrature scheme[57] with 40×146 grid points (per atom).

Geometry optimizations were performed by using the ωB97X-V density functional[58] with the def2-TZVP basis set (all electron for light atoms (through Kr) and with def2-ECP for heavier atoms).[59] The ωB97X-V functional performs very well for both main group[28,60]

and transition metal compounds.[61,62] Vibrational frequency calculations, to confirm minima on the potential energy surface, were computed at the same level of theory. Wavefunctions, energies and orbital localizations were also evaluated at the same level. All DFT calculations were performed with the Q-Chem package,[55] while the OSLO analysis was performed with both the Hilbert space and real-space implementations described above.

Results and Discussion

We evaluate the performance of the OSLO approach for a number of challenging systems, including high-valent oxides, TMs with non-innocent ligands, sulfur dioxide adducts with different bonding patterns, a Zn-based porphyrinic system and TM carbenes of different types (Schrock, Fischer and Grubbs 1st and 2nd generation). We apply both IAO-AutoSAD and TFVC atomic population schemes, to test the robustness of the OSLO procedure to the definition of fragment charges. The full set of results obtained are summarized in Table 1. The OS of the TM and the relevant ligand are reported, together with the FOLI values of the last selected OSLO, which is the least localized one (i.e. largest FOLI value among all selected OSLOs). In fact, once $n_{\mathrm{occ}} - 1$ localized orbitals have been projected out from the density matrix, there is only one (localized) orbital left. This last OSLO is associated with the fragment with the smallest FOLI value.

In many cases the last FOLI value is close to its smallest value of 1, indicating very good orbital localization and, consequently, a clear-cut OS assignment. In cases where the last FOLI value is larger than 1, it is very instructive to examine the Δ-FOLI value (the difference between the smallest and second smallest FOLI values) to see how clear-cut the OS assignment is: the larger the better. Cases with Δ-FOLI > 1 suggest clear-cut ionic character. Overall, the formal OS assignments using both fragment charge schemes agree in almost all cases (30 out of 33). The very few discordant cases have associated Δ-FOLI values below 0.2, which is probably smaller than can be meaningfully associated with application

Table 1: Summary of the OSLO results for the molecular systems studied, obtained with the IAO-AutoSAD and TFVC (in parenthesis) population analysis. OS for TM and selected ligand (L) in bold. tBu = tert-butyl, Cp = cyclopentadienyl, Ar = 2,6-diisopropylphenyl, Ar^1 = 2,6-dimethylphenyl, Cy = cyclohexyl, IMes = 1,3-Dimesitylimidazol-2-ylidene. $^{(a)}$ IAO-AutoSAD alternative solution. $^{(b)}$ TFVC results using tolerance value of 10^{-4}.

Complex	M OS	L OS	Δ-FOLI	Last FOLI
[Ti**O**$_2$]	+4 (+4)	-2 (-2)	3.453 (3.367)	1.321 (1.372)
[V**O**$_4$]$^{3-}$	+5 (+5)	-2 (-2)	1.548 (1.748)	1.466 (1.461)
[Fe**O**$_4$]$^{2-}$	+6 (+6)	-2 (-2)	1.598 (1.682)	1.569 (1.623)
[Re**O**$_4$]$^{-}$	+7 (+7)	-2 (-2)	1.806 (1.829)	1.470 (1.480)
[Os**O**$_4$]	+8 (+8)	-2 (-2)	1.415 (1.363)	1.592 (1.609)
[Ir**O**$_4$]$^{+}$	+9 (+9)	-2 (-2)	1.529 (1.084)	1.705 (1.742)
[Pt**O**$_4$]$^{2+(a)}$	+10 (+10)	-2 (-2)	1.023 (0.707)	1.859 (1.904)
Fe**Cp**$_2$	+2 (+2)	-1 (-1)	1.800 (2.343)	1.313 (1.437)
Zn(**porphyrin**)	+2 (+2)	-2 (-2)	0.958 (1.470)	1.509 (1.319)
[Ni(**S**$_2$**C**$_2$**Me**$_2$)$_2$]^0	+2 (+2)	-1 (-1)	0.000 (0.000)	2.000 (2.245)
[Ni(**S**$_2$**C**$_2$**Me**$_2$)$_2$]$^{1-}$ α	+2 (+3)	-1.5 (-2)	0.603 (0.913)	1.634 (1.656)
[Ni(**S**$_2$**C**$_2$**Me**$_2$)$_2$]$^{1-}$ β			0.000 (0.110)	2.000 (1.901)
[Ni(**S**$_2$**C**$_2$**Me**$_2$)$_2$]$^{2-}$	+2 (+2)	-2 (-2)	1.085 (1.374)	1.482 (1.509)
[Cu(**CF**$_3$)$_4$]$^{1-}$	+3 (+3)	-1 (-1)	0.373 (0.728)	1.516 (1.531)
[Cu(**CF**$_3$)$_4$]$^{2-}$ α	+2 (+2)	-1 (-1)	4.823 (4.845)	1.075 (1.152)
[Cu(**CF**$_3$)$_4$]$^{2-}$ β		-1 (-1)	2.528 (2.867)	1.267 (1.270)
[Cu(**CF**$_3$)$_4$]$^{3-}$	+1 (+1)	-1 (-1)	4.383 (4.581)	1.084 (1.145)
Rh(**SO**$_2$)Cl(PH$_3$)$_2$ (L-type)	+1 (+1)	0 (0)	1.421 (1.209)	1.402 (1.509)
Rh(**SO**$_2$)Cl(CO)(PH$_3$)$_2$ (Z-type)	+1 (+1)	0 (0)	1.064 (1.688)	1.606 (1.516)
Ru(**SO**$_2$)Cl(NO)(PH$_3$)$_2$ (π-type) $^{(b)}$	0 (0)	0 (0)	0.514 (0.339)	2.432 (2.550)
[Fe(CN)$_5$**NO**]$^{2-}$	+2 (+2)	+1 (+1)	0.981 (0.802)	1.573 (1.827)
[Fe(CN)$_5$**NO**]$^{3-}$ α	+2 (+2)	0 (0)	0.839 (0.674)	1.688 (1.987)
[Fe(CN)$_5$**NO**]$^{3-}$ β			2.638 (2.162)	1.375 (1.436)
(CO)$_5$W=**CHN(CH$_3$)$_2$** (1) (Fischer)	0 (0)	0 (0)	3.069 (2.205)	1.920 (3.196)
(CO)$_5$W=**CHOCH$_3$** (2) (Fischer)	0 (0)	0 (0)	1.860 (1.148)	2.037 (3.311)
(CO)$_5$W=**CF**$_2$ (3) (Fischer)	0 (0)	0 (0)	1.567 (0.893)	2.017 (3.232)
(CO)$_5$W=**CH**$_2$ (4) (Fischer)	0 (+2)	0 (-2)	0.612 (0.194)	2.279 (3.142)
NAr(OtBu)$_2$W=**CHtBu** (5) (Schrock)	+6 (+6)	-2 (-2)	0.283 (0.659)	1.924 (1.933)
NAr(OtBu)$_2$W=**CH**$_2$ (6) (Schrock)	+6 (+6)	-2 (-2)	0.455 (0.806)	1.845 (1.908)
NAr^1(OtBu)$_2$Mo=**CHCMe$_2$Ph** (7) (Schrock)	+6 (+6)	-2 (-2)	0.253 (0.565)	1.916 (1.917)
NAr^1(OtBu)$_2$Mo=**CH**$_2$ (8) (Schrock)	+6 (+6)	-2 (-2)	0.203 (0.487)	1.956 (2.018)
NAr^1(OtBu)$_2$Mo=**CHPh** (9) (Schrock)	+6 (+6)	-2 (-2)	0.153 (0.430)	1.986 (2.042)
PCy$_3$Cl$_2$Os=**CH**$_2$ (10) (Grubbs)	+2 (+4)	0 (-2)	0.048 (0.044)	2.089 (2.278)
H$_2$IMesCl$_2$Os=**CH**$_2$ (11) (Grubbs)	+4 (+4)	-2 (-2)	0.192 (0.259)	2.375 (2.709)
PCy$_3$Cl$_2$Ru=**CH**$_2$ (12) (Grubbs)	+2 (+2)	0 (0)	0.222 (0.150)	1.964 (2.199)
H$_2$IMesCl$_2$Ru=**CH**$_2$ (13) (Grubbs)	+2 (+2)	0 (0)	0.276 (0.306)	2.013 (2.149)
(PH$_3$)$_2$Cl$_2$Ru=**CH**$_2$ (14) (Grubbs)	+2 (+2)	0 (0)	0.241 (0.090)	1.961 (2.153)

of the ionic approximation (this will be discussed more later).

We will discuss a few of the more clear-cut cases only briefly. For the high-valent oxides ranging from TiO_2 to IrO_4^+, the OS obtained with OSLO are in full agreement with LOBA, EOS and also with IUPAC's ionic approximation.[35] Clear-cut formal oxo (O^{2-}) ligands are obtained in all cases, resulting in OS as high as Ir(+9).

The PtO_4^{2+} system deserves particular attention. We treat the case of the spin-restricted solution, which is stable in orbital space, and leads to the optimized T_d geometry. There are lower energy spin-polarized solutions but we do not consider them here. The valence MO diagram can be found elsewhere;[63] there are eight π and four σ-type doubly-occupied MOs. In a T_d environment, the $5d$ orbitals of Pt split into E and T_2 symmetries, while the 6s orbital is A_1. The four symmetry-equivalent O atoms lead to σ- and π-type symmetry-adapted orbitals, with symmetries $\Gamma_\sigma = A_1 + T_2$ and $\Gamma_\pi = E + T_1 + T_2$. Towards the end of the iterative procedure, the E type OSLOs on Pt are very close in FOLI with the eight Γ_π of the O centers, due to the significant covalent character of the Pt-O bonds. When using TFVC, the FOLI value of O atoms (1.67) is smaller than that of Pt's E OSLOs (1.84), so they are selected and projected out of the P matrix for the next iteration. Since there is only one set of E orbitals in the occupied space, the aforementioned E-type OSLOs on Pt are now absent, and the OSLOs with smaller FOLI value become those corresponding to the Γ_σ of the O centers, leading to a fairly clear Pt(+10) assignment (see Table 1).

When using IAO-AutoSAD, however, at the same step of the process the situation is reversed. The FOLI value of the Pt E OSLOs is smaller (1.50) than that of the eight Γ_π (1.69). When the former are selected and projected out from the P-matrix, the eight π-type OSLOs of the O centers become rank deficient for the next iterations. This leads to two undesirable outcomes. First, the localized orbitals on the O are mixed-up by the canonical orthogonalization process. Second, a last OSLO of A_1 symmetry delocalized over the four O centers remains left in the last iteration, leading to a huge FOLI value (4.63) and a split of the electron pair among the four equivalent O centers. By applying the branching option

on the IAO-AutoSAD calculation, the Pt(+10) picture obtained with TFVC is recovered, with similar Δ-FOLI value. Selecting OSLOs with a higher FOLI value at a given step of the iterative process ends up providing a final solution where the *sum* of the FOLI values of the selected OSLOs is smaller (36.34 vs 33.22).

The Zn-porphyrin system is potentially challenging for OSLO because, due to its symmetry, the center of charge of the porphyrin ligand *exactly* coincides with the position of the Zn nucleus. Nevertheless, as a result of using the FOLI values, the OSLO procedure performs smoothly, yielding the expected Zn (+2) OS with Δ-FOLI value close to or even larger (TFVC) than 1. The OSLO results for the nitroprusside anion ($[Fe(CN)_5NO]^{2-}$) and its reduced form are also very clear, leading to a formal Fe(+2) species and a ligand-based reduction, in line with the well-known non-innocent nature of the nitrosyl ligand. The IAO-AutoSAD population yields larger Δ-FOLI values as compared to TFVC.

Ferrocene (see Figure 3) is a nice example because it shows the utility of the OSLOs themselves. The cyclopentadienyl anion OSLOs are shown in panels (a) through (c), and the fragment localized π orbitals are particularly pleasing because they resemble the delocalized π orbitals of the isolated anion. In other words, this shows the advantage of *fragment* localization over *global* localization (see also the recent treatment via intrinsic fragment orbitals[44]). The 3 occupied Fe (3d) orbitals emerge as expected, and the OS assignment is very clear based on the small FOLI value of the last orbital as well as the large Δ-FOLI gap.

The redox series of nickel diothiolate complexes, $[Ni(S_2C_2Me_2)_2]^{n-}$ with $n = 0, 1, 2$, is particularly interesting. The $n = 0$ complex is a closed shell singlet. Figure 4 gathers the most relevant OSLOs and the corresponding FOLI values. For Ni, four well-localized d-type orbitals (Figure 4a) are obtained, leading to a Ni(+2) OS. Then, for each thiolate ligand, one finds two S lone pairs and two σ-type orbitals associated with the two S-Ni σ bonds (see Figure 4b). Since each thiolate is a fragment, these two sets of orbitals are not localized into individual S lone pair and S-Ni bonds, but form two in-phase (+,+) and out-of-phase (+,-) localized orbitals within the fragment. The $\sigma(+,-)$ OSLO exhibits a relatively large FOLI

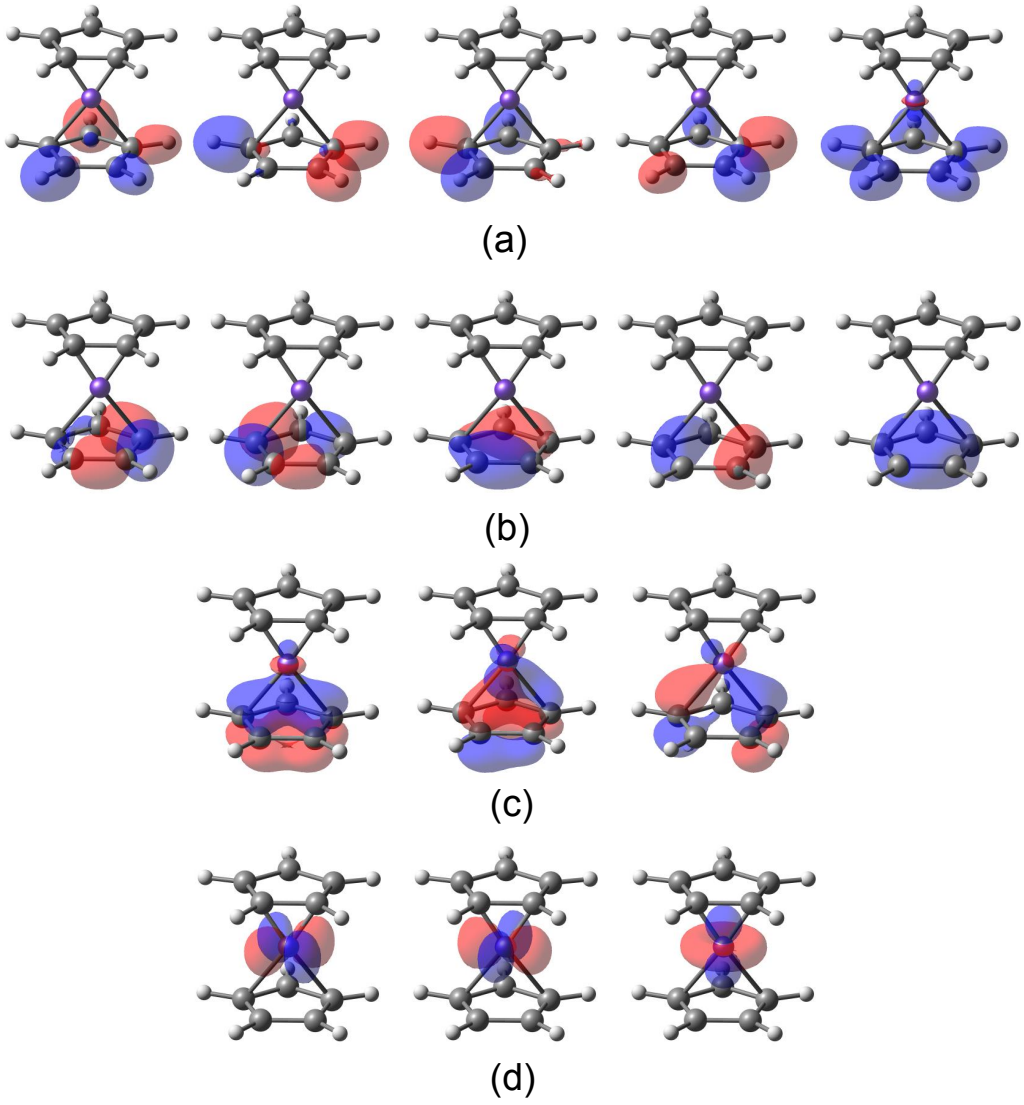

Figure 3: Valence OSLOs for the $FeCp_2$ complex as produced by the algorithm shown in Figure 1. The lower cyclopentadienyl ligand's σ_{C-H} OSLOs are shown in panel (a), its σ_{C-C} OSLOs are shown in panel (b), and its π OSLOs in panel (c). The 3 d-type OSLOs on Fe are shown in panel (d). The isosurface value is 0.075 a.u.

value (~ 1.7), indicating some partial contribution from the Ni center. The $\sigma(+,+)$ orbital shows a minor Ni contribution, leading to a smaller FOLI value (~ 1.3). In addition, each thiolate exhibits a well localized π-type orbital on the two sp^2 carbon atoms, with FOLI ~ 1. The last OSLO, in Figure 4b (bottom right), corresponds to a π-type orbital delocalized over the two thiolate ligands, consistent with the FOLI value (~ 2). Moreover, the Δ-FOLI value is *exactly* zero for both population schemes. This indicates a formal split of the electron pair between the two ligands (in other words, a covalent assignment), leading to two thiolate (-1) moieties to accompany the Ni (+2) center. We can envisage similar situations with the OSLO procedure when dealing with mixed-valence compounds. Visual inspection of the critical localized orbital/s will confirm or deny mixed valence or covalent character suggested by very small Δ-FOLI values.

The two-electron reduction of $[Ni(S_2C_2Me_2)_2]$ leads to the S = 0 closed-shell species $[Ni(S_2C_2Me_2)_2]^{2-}$. The OSLO procedure yields essentially the same valence localized orbitals as in the previously discussed oxidized form (i.e. four d-type localized orbitals on Ni, two lone pairs and two σ type S-Ni orbitals), except that the last delocalized orbital is replaced by two well-localized π-type orbitals, one on each thiolate ligand, as shown in Figure 4c. The Δ-FOLI value is larger than 1, clearly pointing to ligand-based reduction, and in turn, Ni (+2) and two thiolate (-2) moieties.

One-electron reduction to $[Ni(S_2C_2Me_2)_2]^{1-}$ is more tricky. The system is an open-shell doublet ($S = \frac{1}{2}$), and the α and β parts are treated separately. The α part is rather clear cut, yielding similar localized orbitals as in the fully reduced $n = 2$ species, with Δ-FOLI > 0.6. For the β part, using IAO-AutoSAD populations leads to localized orbitals comparable to those of the oxidized form ($n = 0$): four d orbitals on Ni and a last π orbital delocalized over the two thiolate moieties, with FOLI ~ 2 and Δ-FOLI= 0. These OLSOs suggest a mixed-valence situation with Ni(+2) and two partially-reduced thiolates (-1.5), from equal sharing of the last beta electron between the thiolates. This result, as well as those for the closed-shell species, agrees with the experimental evidence[64,65] and with the EOS scheme.[35]

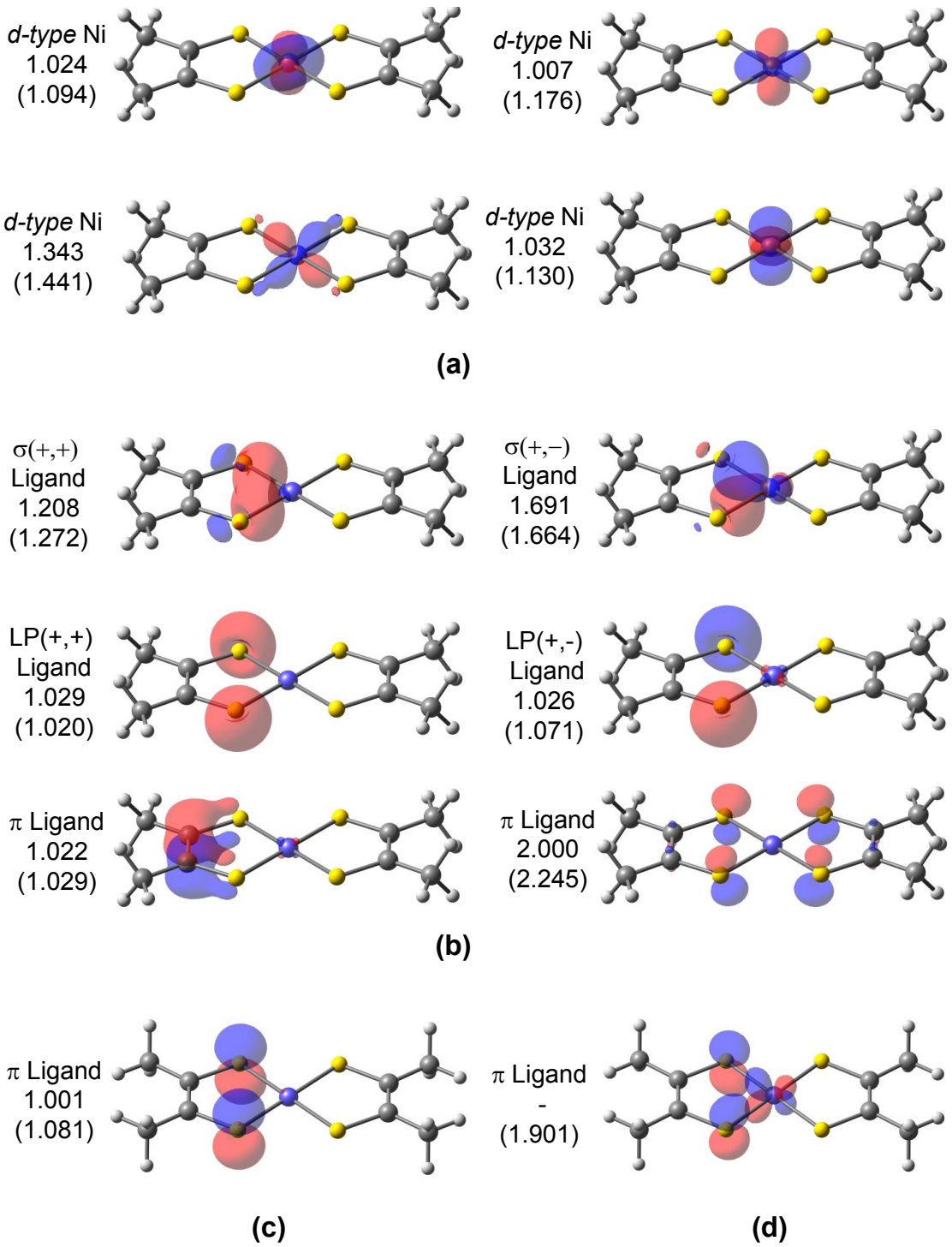

Figure 4: Valence LOs of the $[Ni(S_2C_2Me_2)_2]^0$ system with IAO-AutoSAD and TFVC (in parenthesis) FOLI values. *d*-type orbitals on Ni (a), ligand's σ, lone pair (LP) and π obitals (b). Last localized ligand π orbital for $[Ni(S_2C_2Me_2)_2]^{2-}$ (c). Last localized ligand π orbital from the beta density of $[Ni(S_2C_2Me_2)_2]^-$ using TFVC (d). The isosurface value is 0.075 a.u.

However, the results for the β part of the $S = \frac{1}{2}$ species are somewhat different when using TFVC populations. In the iterative process, two equivalent π-type orbitals centered on each thiolate with significant contribution from the Ni center (see Figure 4d) are selected over the d-type orbital centered on Ni (which also exhibits significant mixing with the ligands). The FOLI values are 1.901 and 2.011, respectively, indicating a large degree of delocalization of these last orbitals. As a consequence, the picture obtained is a Ni(+3) with two fully reduced thiolate (-2) ligands, with a Δ-FOLI value of merely 0.11. This very small Δ-FOLI value argues for equal sharing of the last electron pair.

In Naumann's ion,[66] $[Cu(CF_3)_4]^-$, Cu OS and role of the CF_3 ligands has been debated for more than 25 years.[67–72] Based on the DFT frontier molecular orbitals, Snyder considered that the metal center is best described as Cu (+1) (i.e. d^{10}), instead of a d^8 Cu (+3) as would follow if all CF_3 ligands were formally anionic (-1).[67] According to Snyder, the anion features an "inverted" ligand field,[72] where the lowest unoccupied molecular orbital (LUMO) exhibits dominant ligand character. This assignment has been questioned by others, who support the latter, more conventional, view of four CF_3^- ligands.[68,69] Most recently, the Lancaster group have put forward further experimental and computational arguments in favor of d^{10}.[70,71] Other arguments supporting the Cu (+1) and Cu (+3) picture have also been given.[72]

These conflicting views are rooted in the relatively non-polar character of the Cu-C bond. In recent work, some of us showed that both the LOBA and EOS schemes give OS assignments consistent with a formal Cu (+3) species.[35] While the LOBA results were rather clear, the R (%) = 51.7 value of the EOS assignment indicated a very close call. The OSLO procedure (with either population analysis) points towards formal anionic CF_3 (-1) ligands and hence a Cu (+3) species, as shown on Table 1. One can identify four well-localized d-type orbitals centered on Cu (Figure 5a), while the σ-type interaction between Cu and each CF_3 is captured by four equivalent ligand-centered orbitals with non-negligible contribution from the Cu (Figure 5b). Notice also the mixing of p-type orbitals from the F atoms of the CF_3 moiety. These localized orbitals provide a much clearer picture as compared to those

obtained with PM localization for the same wavefunction.[35] Encouragingly. the FOLI values of the last orbitals are virtually the same with both atomic population schemes ($\sim$ 1.5). The Δ-FOLI value for the assignment is somewhat smaller using IAO-AutoSAD (0.373) as compared to TFVC (0.728), but the same picture emerges in both cases. Finally, OSLO results for the one- and two-electron reduction of $[Cu(CF_3)_4]^-$ indicate that both processes are metal based, as expected given the Cu (+3) assignment of the anion.

In TM carbenes a double bond is formed between the TM and the carbene. The σ bond is understood as originating from σ-donation of a sp^2 lone pair on the carbon atom to the TM. The nature of the π-type interaction is much more system-dependent, leading to two well-established situations. In the so-called Fischer carbenes, the π electrons formally sit on the TM d-type orbital, which back-donates to a formally neutral carbene moiety. In Schrock-type carbenes, the π electrons are formally associated with the carbene moiety, which becomes anionic (-2). Previous experience indicated that OS assignment in TM-carbene complexes is challenging. Often, EOS analysis yields low R(%) values rather close to 50, driven by nearly equal populations of the π-type EFOs on the TM and the carbene moiety. With LOBA, Pipek-Mezey localized orbitals do not readily correspond with the σ and π bonds.[35] We studied a set of fourteen TM carbenes.[73] The set includes four conventional W-based Fischer carbenes (1–4), five Schrock W- and Mo-based catalysts (5–9) and five Ru- and Os-based 1st and 2nd generation Grubbs catalysts (10–14).

Referring again to Table 1, the OSLO procedure combined with IAO-AutoSAD populations correctly identifies all prototypical Fischer and Schrock carbenes, while all Grubbs catalysts but 10 are pictured as formal neutral Fisher-type carbenes. Notice the Δ-FOLI values are mostly below 0.3 (especially for nominal Schrock and Grubbs carbenes), with FOLI values around 2.0, indicating significant delocalization of the last orbital. Such values could support a covalent division of charge, and, at the very least, call for inspection of the relevant σ-type and π-type TM-carbene OSLOs. To this end, Figure 6 shows two examples of OSLOs involving the TM and the carbene unit. The FOLI values of the σ-type bonds (left)

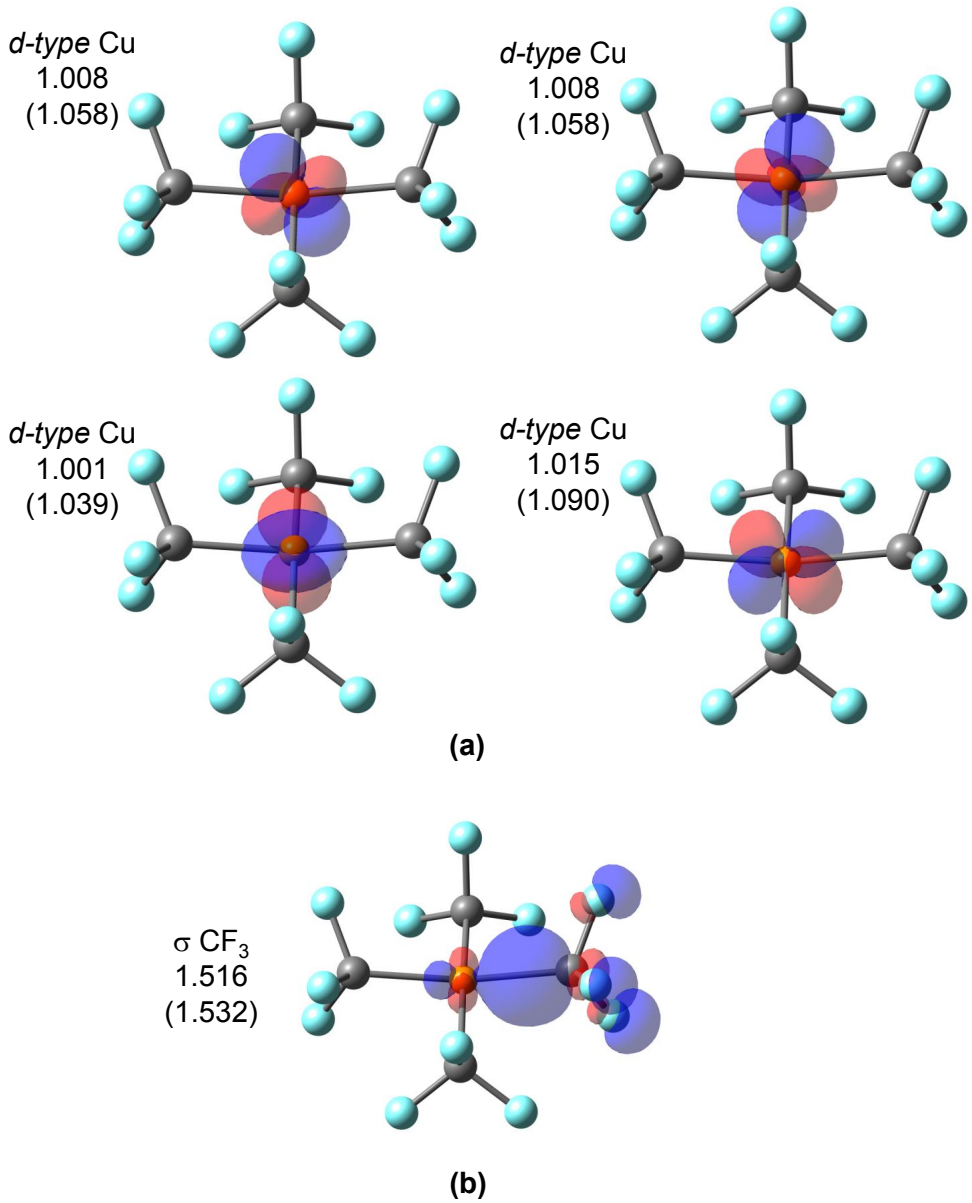

Figure 5: Selected LOs of $[Cu(CF_3)_4]^-$ with IAO-AutoSAD and TFVC (in parenthesis) FOLI values for Cu (a) and the CF_3 ligand (b). The relatively non-polar character of the σ Cu-CF_3 interaction is clearly evident. However the FOLI value (~ 1.5) as well as visual inspection indicates that this orbital has greater $CF_3{}^-$ character than Cu (3d) character so that in a winner-take-all assignment, the ligands emerge as $CF_3{}^-$ and the metal adopts a Cu (+3) OS. The isosurface value for the plots is 0.075 a.u.

are noticeably smaller than those of the π-type bonds (right), which exhibit a very similar contribution from both fragments. Yet, one can see that the OSLO procedure produces nice, chemically interpretable localized orbitals for the σ and π bonding.

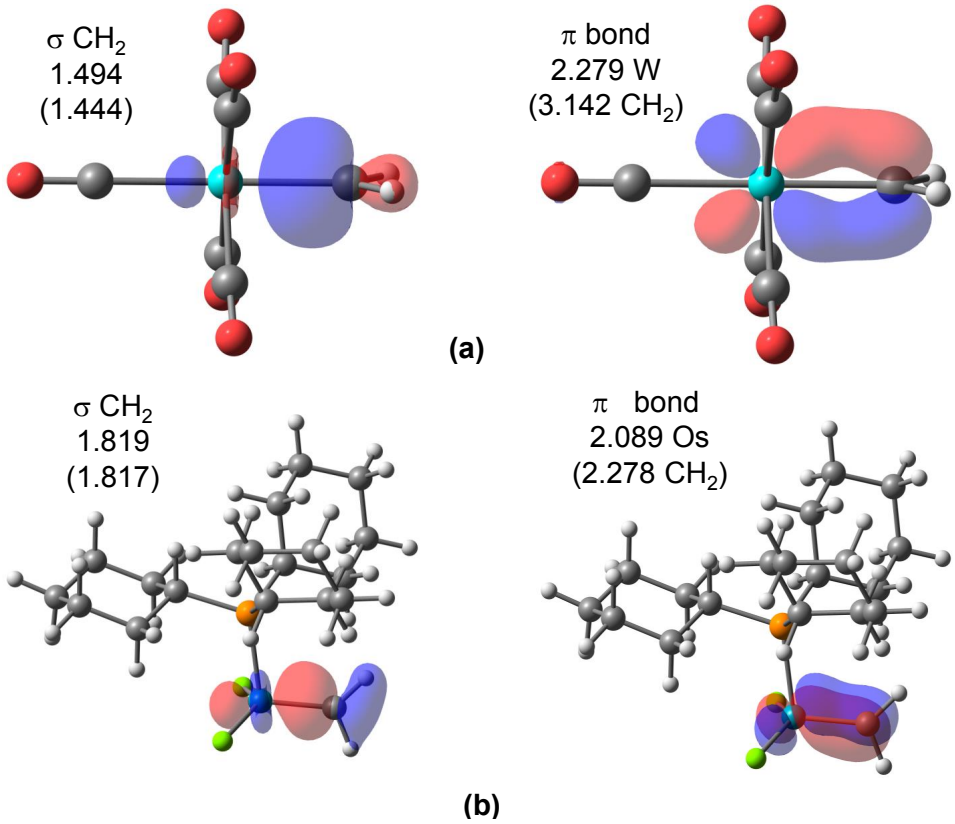

Figure 6: σ and π TM-carbene OSLOs for (a) the Fischer-type $(CO)_5W{=}\mathbf{CH}_2$ complex (species 4), and (b) the Grubbs-type $PCy_3Cl_2Os{=}\mathbf{CH}_2$ complex (species 10). The FOLI values for each orbital are shown using IAO-AutoSAD (with the corresponding TFVC values in parentheses). The large FOLI values (> 2) for the π-type TM-carbene interaction, as well as visual inspection show the shared electron character of this interaction. The isosurface value is 0.075.

For the two cases shown in Figure 6, the IAO-AutoSAD and TFVC fragment charges lead to different OS assignments, despite yielding almost identical sets of localized orbitals. The σ-type OSLO belongs to the carbene, with FOLI values of ~ 1.5 and ~ 1.8 for the Fischer-type $(CO)_5W{=}\mathbf{CH}_2$ complex (4), and the Grubbs-type $PCy_3Cl_2Os{=}\mathbf{CH}_2$ complex (10), respectively. The π-type OSLO is the origin of the discrepancy. Since this is the last selected orbital in the OSLO procedure, its allegiance is based on the FOLI values for each fragment. In the case of 10, TFVC provides FOLI values of 2.28 for the carbene and 2.32 for the TM, while for IAO-AutoSAD the values are 2.14 and 2.09, respectively. Consequently, ionic assignment leads to a neutral CH_2 according to IAO-AutoSAD and to

an anionic CH_2 (-2) according to TFVC. Notice that Δ-FOLI values are below 0.05 in both cases, the smallest seen in this study. The genuinely covalent nature of this π bond precludes meaningful classification of this system as Fischer or Schrock: instead the electron pair is shared.

On the other hand, the different OS assignment for 4 is rather unexpected, as both population methods produce virtually the same set of OSLOs. With IAO-AutoSAD, (4) is quite clearly a neutral Fischer-type carbene with a Δ-FOLI value of 0.61. However, when using TFVC, the assignment is not only reversed, with a small Δ-FOLI (0.19), but also the FOLI values of the last π-type OSLO are significantly higher (3.14 and 3.34 for the carbene and TM metal, respectively). The fragment TFVC populations on the carbene and the W atom are 0.76 e^- and 0.66 e^-, respectively. Hence, the remaining 0.58 e^- belongs to the spectator CO ligands, which explains the large FOLI value obtained. By contrast, with IAO-AutoSAD, the population of the carbene and W are 0.64 and 1.03 e^-, so the electron pair is more clearly on W (although covalent character is visually evident in Figure 6).

As a last example, let us consider the species described in IUPAC's technical report illustrating three different bonding modes of the SO_2 ligand.[2,3] Karen showed that when acting as a Z-type ligand (i.e. as a Lewis acid), the electronegative-acceptor caveat had to be applied to the ionic approximation so that the SO_2 ligand remains neutral. With EOS analysis the expected neutral SO_2 ligand was recovered in all three cases.[26] The OSLO results of Table 1 also clearly identify a neutral SO_2 moiety for both the L-type and Z-type configurations, with large Δ-FOLI values of over 1.0. In the case of the π-type bonding configuration, the SO_2 is once again clearly identified as neutral, but there is a close-call situation involving Ru and a non-innocent nitrosyl ligand trans to the SO_2, that calls for visual inspection of the OSLOs. The last three OSLOs (from IAO-AutoSAD results) belong to Ru, with FOLI values of 1.44, 1.88 and 2.43, and are depicted in Figure 7. The admixture of contributions from the SO_2 and NO ligands is indeed significant for the last OLSO (Figure 7b), but the Δ-FOLI value of 0.51 suggests that an ionic assignment to Ru remains justified.

Overall, this results in a Ru (0), SO_2 (0) and NO (+1) OS assignment.

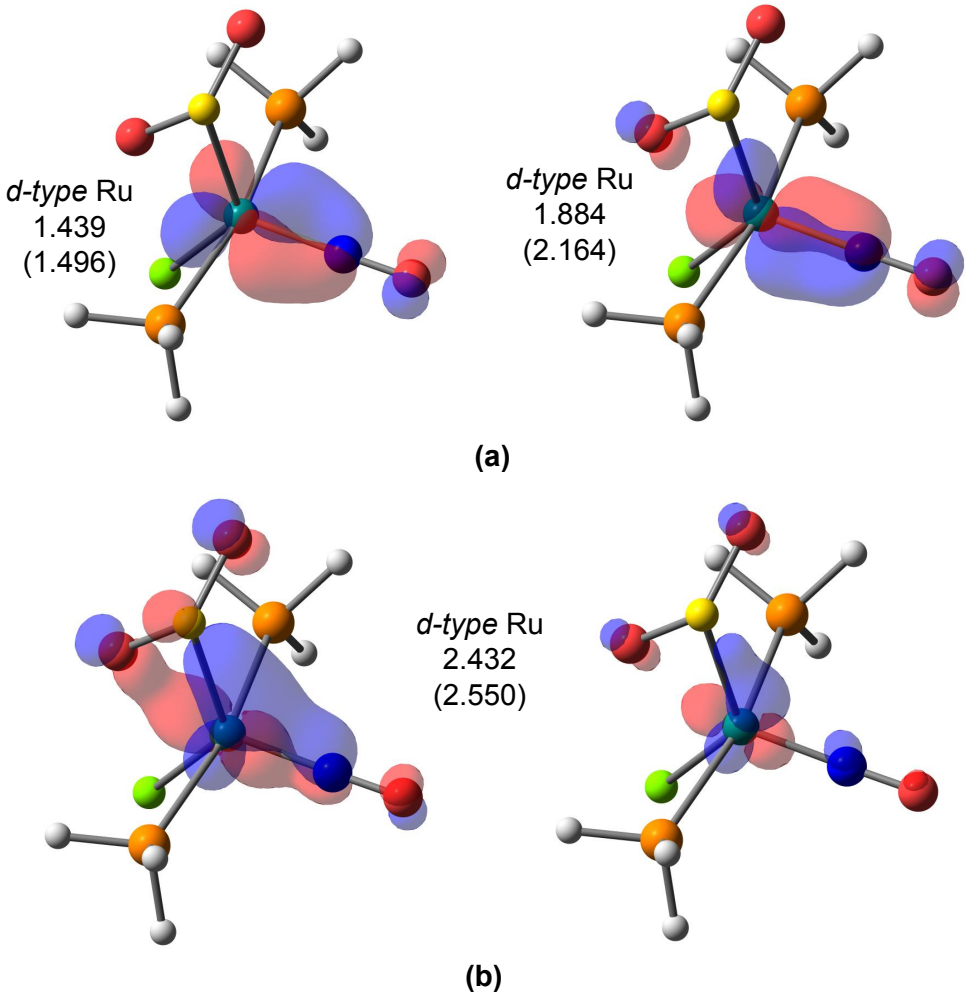

Figure 7: Selected Ru-centered OSLOs for $Ru(SO_2)Cl(NO)(PH_3)_2$ (π-type), with IAO-AutoSAD and TFVC (in parenthesis) FOLI values. The isosurface is 0.075 a.u. for panel (a) which shows the 3rd and 2nd last OSLOs to be selected. In panel (b), which shows the last OSLO selected, there are also significant ligand contributions as evident from the larger FOLI value, and visual inspection of the orbital isosurface of 0.075 a.u. (left), which can be clarified by choosing a larger value of 0.125 a.u. for the isosurface (right).

When using TFVC populations with the default tolerance of 10^{-2}, the last two localized orbitals, one centered on Ru and another on NO, have FOLI values within the tolerance and are therefore selected together in the last step of the iterative procedure, leading to a different OS assignment. However, the linear-dependency check indicates significant overlap between these two orbitals. As a consequence, their shape substantially changes after

orthogonalization, leading to a pair of localized orbitals very similar to those of Figure 7. In this case, being a non-symmetric system, a tighter tolerance of 10^{-4} affords the selection of the last orbitals in the iterative process one by one, readily producing the same results obtained with IAO-AutoSAD.

Conclusions

The purpose of this work was to report a new oxidation state localized orbital (OSLO) scheme that performs orbital localization based on *molecular fragments*, after a DFT calculation with chosen total charge and spin state. The user should select a fragmentation of the target complex, such as separation into one (or more) metal centers and individual ligands. After an iterative process to select the most strongly fragment-localized OSLOs, each molecular fragment is associated with a set of localized orbitals derived from a simple orbital spread criterion. This association, in turn, determines the fragment's formal charge or oxidation state (OS) in a natural manner.

We introduced a new index, namely the fragment orbital localization index (FOLI), to quantify the degree of locality of each OSLO (or any input orbital) on each fragment. As examples, the lowest possible FOLI value of 1 corresponds to complete localization on that fragment, while perfect delocalization between 2 fragments yields a FOLI value of 2. Evaluation of FOLIs requires fragment populations. Two distinct population schemes have been tested for this purpose, namely a real-space approach (TFVC) and a new version of the intrinsic atomic orbitals (IAO-AutoSAD) that uses on-the-fly evaluation of the reference minimal basis based on superposition of atomic densities (SAD).

The OSLO iterative procedure selects the orbital with lowest FOLI value on each iteration, so that the last OSLO produced has the largest FOLI value (and is least strongly fragment-localized) among the whole set. The Δ-FOLI value for the last localized orbital measures the gap with the second smallest FOLI value among the fragments. Δ-FOLI mea-

sures the reliability of the OS assignment, such that a Δ-FOLI value larger than 0.5 usually indicates a clear OS assignment. Smaller values suggest increasingly covalent character in the least localized OSLO.

Numerical tests of the new scheme shows that the OSLOs are in much better agreement with the expected Lewis structure than those obtained with other *global* localization schemes such as Pipek-Mezey (apart from straightforward cases). As a result, previously identified limitations of the localized orbital bonding analysis (LOBA) procedure for OS assignment that originate in the use of global orbital localization methods are overcome with the OSLO approach. Transition metal carbenes are one such class of examples.

The OSLOs themselves carry significant chemical information, and their visualization helps to clarify borderline OS assignments. One such example discussed here is the $Cu(CF_3)_4^-$ anion, where the OSLO corresponding to the $\sigma(Cu-CF_3)$ interaction exhibits some covalent character, but supports a conventional d^8 Cu configuration rather than d^{10}. Another example is the Grubbs catalyst, $PCy_3Cl_2Os{=}CH_2$, where the OSLO corresponding to the Os-carbene π bond is almost perfectly covalent, thus rendering the conventional Fischer and Schrock classifications inapplicable.

We find the IAO-AutoSAD population scheme performs well in combination with OSLO, outperforming the TFVC scheme that is conventionally used in the framework of effective oxidation state (EOS) analysis. IAO-AutoSAD represents a promising all-round general, fast, analytical, basis-set independent Hilbert-space based atomic population scheme.

Associated Content

The Supporting Information is available free of charge at https://pubs.acs.org/doi/xxxx.xxxxx, and contains xyz files for all inputs needed to reproduce the calculations reported herein.

Acknowledgements

M.G. thanks the Generalitat de Catalunya and Fons Social Europeu for the predoctoral fellowship (2018 FI_B 01120). P.S. was supported by the Ministerio de Ciencia, Innovacion y Universidades (MCIU), Grant PGC2018-098212-B-C22. A.A and M.H.G. acknowledge support from the U.S. National Science Foundation through Grant No. CHE-1955643, and additional support from CALSOLV.

References

(1) Karen, P. Oxidation State, A Long-Standing Issue! *Ang. Chem. Int. Ed.* **2015**, *54*, 4716–4726.

(2) Karen, P.; McArdle, P.; Takats, J. Toward a comprehensive definition of oxidation state (IUPAC Technical Report). *Pure Appl. Chem.* **2014**, *86*, 1017–1081.

(3) Karen, P.; McArdle, P.; Takats, J. Comprehensive definition of oxidation state (IUPAC Recommendations 2016). *Pure Appl. Chem.* **2016**, *88*, 831–839.

(4) Lyaskovskyy, V.; de Bruin, B. Redox non-innocent ligands: versatile new tools to control catalytic reactions. *ACS Catal.* **2012**, *2*, 270–279.

(5) Minkin, V. I.; Glukhovtsev, M. N.; Simkin, B. Y. *Aromaticity and antiaromaticity*; John Wiley & Sons, Incorporated, 1994.

(6) Balaban, A. T.; Oniciu, D. C.; Katritzky, A. R. Aromaticity as a cornerstone of heterocyclic chemistry. *Chem. Rev.* **2004**, *104*, 2777–2812.

(7) Boldyrev, A. I.; Wang, L.-S. Beyond organic chemistry: aromaticity in atomic clusters. *Phys. Chem. Chem. Phys.* **2016**, *18*, 11589–11605.

(8) Heitkemper, T.; Sarcevic, J.; Sindlinger, C. P. A Neutral Silicon(II) Half-Sandwich Compound. *J. Am. Chem. Soc.* **2020**, *142*, 21304–21309.

(9) Min, X.; Popov, I. A.; Pan, F.-X.; Li, L.-J.; Matito, E.; Sun, Z.-M.; Wang, L.-S.; Boldyrev, A. I. All-Metal Antiaromaticity in Sb4-Type Lanthanocene Anions. *Ang. Chem. Int. Ed.* **2016**, *55*, 5531–5535.

(10) Panetier, J. A.; Letko, C. S.; Tilley, T. D.; Head-Gordon, M. Computational Characterization of Redox Non-Innocence in Cobalt-Bis(Diaryldithiolene)-Catalyzed Proton Reduction. *J. Chem. Theory Comput.* **2016**, *12*, 223–230.

(11) Raebiger, H.; Lany, S.; Zunger, A. Charge self-regulation upon changing the oxidation state of transition metals in insulators. *Nature* **2008**, *453*, 763–766.

(12) Resta, R. Charge states in transition. *Nature* **2008**, *453*, 735–735.

(13) Steen, J. S.; Knizia, G.; Klein, J. E. M. N. σ-Noninnocence: Masked Phenyl-Cation Transfer at Formal NiIV. *Ang. Chem. Int. Ed.* **2019**, *58*, 13133–13139.

(14) Walsh, A.; Sokol, A. A.; Buckeridge, J.; Scanlon, D. O.; Catlow, C. R. A. Electron Counting in Solids: Oxidation States, Partial Charges, and Ionicity. *J. Phys. Chem. Lett.* **2017**, *8*, 2074–2075.

(15) Ampßler, T.; Monsch, G.; Popp, J.; Riggenmann, T.; Salvador, P.; Schröder, D.; Klüfers, P. Not Guilty on Every Count: The "Non-Innocent" Nitrosyl Ligand in the Framework of IUPAC's Oxidation-State Formalism. *Ang. Chem. Int. Ed.* **2020**, *59*, 12381–12386.

(16) Wang, G.; Zhou, M.; Goettel, J. T.; Schrobilgen, G. J.; Su, J.; Li, J.; Schlöder, T.; Riedel, S. Identification of an iridium-containing compound with a formal oxidation state of IX. *Nature* **2014**, *514*, 475–477.

(17) Thom, A. J. W.; Sundstrom, E. J.; Head-Gordon, M. LOBA: a localized orbital bonding analysis to calculate oxidation states, with application to a model water oxidation catalyst. *Phys. Chem. Chem. Phys.* **2009**, *11*, 11297–11304.

(18) Sit, P. H.-L.; Zipoli, F.; Chen, J.; Car, R.; Cohen, M. H.; Selloni, A. Oxidation State Changes and Electron Flow in Enzymatic Catalysis and Electrocatalysis through Wannier-Function Analysis. *Chem. Eur. J.* **2011**, *17*, 12136–12143.

(19) Ramos-Cordoba, E.; Postils, V.; Salvador, P. Oxidation States from Wave Function Analysis. *J. Chem. Theory Comput.* **2015**, *11*, 1501–1508.

(20) Gimferrer, M.; Comas-Vilà, G.; Salvador, P. Can We Safely Obtain Formal Oxidation States from Centroids of Localized Orbitals? *Molecules* **2020**, *25*, 234.

(21) Catlow, C. R. A.; Stoneham, A. M. Ionicity in solids. *J. Phys. C* **1983**, *16*, 4321.

(22) Jiang, L.; Levchenko, S. V.; Rappe, A. M. Rigorous definition of oxidation states of ions in solids. *Phys. Rev. Lett.* **2012**, *108*, 166403.

(23) Walsh, A.; Sokol, A. A.; Buckeridge, J.; Scanlon, D. O.; Catlow, C. R. A. Oxidation states and ionicity. *Nature Mat.* **2018**, *17*, 958–964.

(24) Mayer, I. Relation between the Hilbert space and "fuzzy atoms" analyses. *Chem. Phys. Lett.* **2013**, *585*, 198–200.

(25) Ramos-Cordoba, E.; Salvador, P.; Mayer, I. The atomic orbitals of the topological atom. *J. Chem. Phys.* **2013**, *138*, 214107.

(26) Postils, V.; Delgado-Alonso, C.; Luis, J. M.; Salvador, P. An Objective Alternative to IUPAC's Approach To Assign Oxidation States. *Ang. Chem. Int. Ed.* **2018**, *57*, 10525–10529.

(27) Høyvik, I.-M.; Jørgensen, P. Characterization and generation of local occupied and virtual Hartree–Fock orbitals. *Chem. Rev.* **2016**, *116*, 3306–3327.

(28) Mardirossian, N.; Head-Gordon, M. Thirty years of density functional theory in computational chemistry: an overview and extensive assessment of 200 density functionals. *Mol. Phys.* **2017**, *115*, 2315–2372.

(29) Boys, S. F. Construction of Some Molecular Orbitals to Be Approximately Invariant for Changes from One Molecule to Another. *Rev. Mod. Phys.* **1960**, *32*, 296–299.

(30) Edmiston, C.; Ruedenberg, K. Localized Atomic and Molecular Orbitals. *Rev. Mod. Phys.* **1963**, *35*, 457–464.

(31) Pipek, J.; Mezey, P. G. A fast intrinsic localization procedure applicable for ab initio and semiempirical linear combination of atomic orbital wave functions. *J. Chem. Phys.* **1989**, *90*, 4916–4926.

(32) Aquilante, F.; Bondo Pedersen, T.; Sánchez de Merás, A.; Koch, H. Fast noniterative orbital localization for large molecules. *J. Chem. Phys.* **2006**, *125*, 174101.

(33) Høyvik, I.-M.; Jansik, B.; Jørgensen, P. Orbital localization using fourth central moment minimization. *J. Chem. Phys.* **2012**, *137*, 224114.

(34) Knizia, G. Intrinsic Atomic Orbitals: An Unbiased Bridge between Quantum Theory and Chemical Concepts. *J. Chem. Theory Comput.* **2013**, *9*, 4834–4843.

(35) Gimferrer, M.; Van der Mynsbrugge, J.; Bell, A. T.; Salvador, P.; Head-Gordon, M. Facing the Challenges of Borderline Oxidation State Assignments Using State-of-the-Art Computational Methods. *Inorg. Chem.* **2020**, *59*, 15410–15420.

(36) Stoll, H.; Wagenblast, G.; Preuss, H. On the use of local basis-sets for localized molecular-orbitals. *Theor. Chim. Acta* **1980**, *57*, 169–178.

(37) Raimondi, M.; Famulari, A.; Specchio, R.; Sironi, M.; Moroni, F.; Gianinetti, E. Ab initio non-orthogonal approaches to the computation of weak interactions and of localised molecular orbitals for QM/MM procedures. *J. Mol. Struct. Theochem* **2001**, *573*, 25–42.

(38) Nagata, T.; Takahashi, O.; Saito, K.; Iwata, S. Basis set superposition error free self-consistent field method for molecular interaction in multi-component systems: Projection operator formalism. *J. Chem. Phys.* **2001**, *115*, 3553–3560.

(39) Khaliullin, R. Z.; Head-Gordon, M.; Bell, A. T. An efficient self-consistent field method for large systems of weakly interacting components. *J. Chem. Phys.* **2006**, *124*, 204105.

(40) Sax, A. F. Localization of molecular orbitals on fragments. *J. Comput. Chem.* **2012**, *33*, 1495–1510.

(41) de Silva, P.; Giebułtowski, M.; Korchowiec, J. Fast orbital localization scheme in molecular fragments resolution. *Phys. Chem. Chem. Phys.* **2012**, *14*, 546–552.

(42) Horn, P. R.; Sundstrom, E. J.; Baker, T. A.; Head-Gordon, M. Unrestricted absolutely localized molecular orbitals for energy decomposition analysis: Theory and applications to intermolecular interactions involving radicals. *J. Chem. Phys.* **2013**, *138*, 134119.

(43) Li, Z.; Li, H.; Suo, B.; Liu, W. Localization of molecular orbitals: from fragments to molecule. *Acc. Chem. Res.* **2014**, *47*, 2758–2767.

(44) Senjean, B.; Sen, S.; Repisky, M.; Knizia, G.; Visscher, L. Generalization of Intrinsic Orbitals to Kramers-Paired Quaternion Spinors, Molecular Fragments, and Valence Virtual Spinors. *J. Chem. Theory Comput.* **2021**, *17*, 1337–1354.

(45) Mo, Y.; Bao, P.; Gao, J. Energy decomposition analysis based on a block-localized wavefunction and multistate density functional theory. *Phys. Chem. Chem. Phys.* **2011**, *13*, 6760–6775.

(46) Mao, Y.; Loipersberger, M.; Horn, P. R.; Das, A.; Demerdash, O.; Levine, D. S.; Prasad Veccham, S.; Head-Gordon, T.; Head-Gordon, M. From Intermolecular Interaction Energies and Observable Shifts to Component Contributions and Back Again: A

Tale of Variational Energy Decomposition Analysis. *Ann. Rev. Phys. Chem.* **2021**, *72*, 641–666.

(47) Giovannini, T.; Koch, H. Energy-based molecular orbital localization in a specific spatial region. *J. Chem. Theory Comput.* **2020**, *17*, 139–150.

(48) Subotnik, J. E.; Sodt, A.; Head-Gordon, M. Localized orbital theory and ammonia triborane. *Phys. Chem. Chem. Phys.* **2007**, *9*, 5522–5530.

(49) Pipek, J. Localization measure and maximum delocalization in molecular systems. *Int. J. Quantum Chem.* **1989**, *36*, 487–501.

(50) Salvador, P.; Ramos-Cordoba, E. Communication: An approximation to Bader's topological atom. *J. Chem. Phys.* **2013**, *139*, 071103.

(51) Lee, M. S.; Head-Gordon, M. Extracting polarized atomic orbitals from molecular orbital calculations. *Int. J. Quantum Chem.* **2000**, *76*, 169–184.

(52) Lu, W. C.; Wang, C. Z.; Schmidt, M. W.; Bytautas, L.; Ho, K. M.; Ruedenberg, K. Molecule intrinsic minimal basis sets. I. Exact resolution of ab initio optimized molecular orbitals in terms of deformed atomic minimal-basis orbitals. *J. Chem. Phys.* **2004**, *120*, 2629–2637.

(53) Laikov, D. N. Intrinsic minimal atomic basis representation of molecular electronic wavefunctions. *Int. J. Quantum Chem.* **2011**, *111*, 2851–2867.

(54) Janowski, T. Near equivalence of intrinsic atomic orbitals and quasiatomic orbitals. *J. Chem. Theory Comput.* **2014**, *10*, 3085–3091.

(55) Epifanovsky, E.; Gilbert, A. T.; Feng, X.; Lee, J.; Mao, Y.; Mardirossian, N.; Pokhilko, P.; White, A. F.; Coons, M. P.; Dempwolff, A. L., et al. Software for the frontiers of quantum chemistry: An overview of developments in the Q-Chem 5 package. *J. Chem. Phys.* **2021**, *155*, 084801.

(56) Salvador, P.; Ramos-Cordoba, E.; Gimferrer, M. APOST-3D. 2019; Institute of Computational Chemistry and Catalysis, University of Girona: Girona.

(57) Becke, A. D. A multicenter numerical integration scheme for polyatomic molecules. *J. Chem. Phys.* **1988**, *88*, 2547–2553.

(58) Mardirossian, N.; Head-Gordon, M. ωB97X-V: A 10-parameter, range-separated hybrid, generalized gradient approximation density functional with nonlocal correlation, designed by a survival-of-the-fittest strategy. *Phys. Chem. Chem. Phys.* **2014**, *16*, 9904–9924.

(59) Weigend, F.; Ahlrichs, R. Balanced basis sets of split valence, triple zeta valence and quadruple zeta valence quality for H to Rn: Design and assessment of accuracy. *Phys. Chem. Chem. Phys.* **2005**, *7*, 3297–3305.

(60) Goerigk, L.; Hansen, A.; Bauer, C.; Ehrlich, S.; Najibi, A.; Grimme, S. A look at the density functional theory zoo with the advanced GMTKN55 database for general main group thermochemistry, kinetics and noncovalent interactions. *Phys. Chem. Chem. Phys.* **2017**, *19*, 32184–32215.

(61) Dohm, S.; Hansen, A.; Steinmetz, M.; Grimme, S.; Checinski, M. P. Comprehensive thermochemical benchmark set of realistic closed-shell metal organic reactions. *J. Chem. Theory Comput.* **2018**, *14*, 2596–2608.

(62) Chan, B.; Gill, P. M.; Kimura, M. Assessment of DFT methods for transition metals with the TMC151 compilation of data sets and comparison with accuracies for main-group chemistry. *J. Chem. Theory Comput.* **2019**, *15*, 3610–3622.

(63) Hu, S.-X.; Li, W.-L.; Lu, J.-B.; Bao, J. L.; Yu, H. S.; Truhlar, D. G.; Gibson, J. K.; Marçalo, J.; Zhou, M.; Riedel, S.; Schwarz, W. H. E.; Li, J. On the Upper Limits of Oxidation States in Chemistry. *Ang. Chem. Int. Ed.* **2018**, *57*, 3242–3245.

(64) Davison, A.; Edelstein, N.; Holm, R. H.; Maki, A. H. The Preparation and Characterization of Four-Coordinate Complexes Related by Electron-Transfer Reactions. *Inorg. Chem.* **1963**, *2*, 1227–1232.

(65) Lim, B. S.; Fomitchev, D. V.; Holm, R. H. Nickel Dithiolenes Revisited: Structures and Electron Distribution from Density Functional Theory for the Three-Member Electron-Transfer Series $[Ni(S_2C_2Me_2)_2]^{0,1-,2-}$. *Inorg. Chem.* **2001**, *40*, 4257–4262.

(66) Naumann, D.; Roy, T.; Tebbe, K.-F.; Crump, W. Synthesis and Structure of Surprisingly Stable Tetrakis(trifluoromethyl)cuprate(III) Salts. *Ang. Chem. Int. Ed. 32*, 1482–1483.

(67) Snyder, J. P. Elusiveness of Cu^{III} Complexation; Preference for Trifluoromethyl Oxidation in the Formation of $[Cu^{I}(CF_3)_4]^-$ Salts. *Ang. Chem. Int. Ed.* **1995**, *34*, 80–81.

(68) Kaupp, M.; von Schnering, H. G. Formal Oxidation State versus Partial Charge-A Comment. *Ang. Chem. Int. Ed.* **1995**, *34*, 986–986.

(69) Aullón, G.; Alvarez, S. Oxidation states, atomic charges and orbital populations in transition metal complexes. *Theor. Chem. Acc.* **2009**, *123*, 67–73.

(70) Walroth, R. C.; Lukens, J. T.; MacMillan, S. N.; Finkelstein, K. D.; Lancaster, K. M. Spectroscopic Evidence for a $3d^{10}$ Ground State Electronic Configuration and Ligand Field Inversion in $[Cu(CF_3)_4]^{1-}$. *J. Am. Chem. Soc.* **2016**, *138*, 1922–1931.

(71) DiMucci, I. M.; Lukens, J. T.; Chatterjee, S.; Carsch, K. M.; Titus, C. J.; Lee, S. J.; Nordlund, D.; Betley, T. A.; MacMillan, S. N.; Lancaster, K. M. The Myth of d^8 Copper(III). *J. Am. Chem. Soc.* **2019**, *141*, 18508–18520.

(72) Hoffmann, R.; Alvarez, S.; Mealli, C.; Falceto, A.; Cahill, T. J.; Zeng, T.; Manca, G. From Widely Accepted Concepts in Coordination Chemistry to Inverted Ligand Fields. *Chem. Rev.* **2016**, *116*, 8173–8192.

(73) Occhipinti, G.; Jensen, V. R. Nature of the transition metal-carbene bond in Grubbs olefin metathesis catalysts. *Organometallics* **2011**, *30*, 3522–3529.